# Kinetic evolution of unmixing in an AlLi alloy using x-ray intensity fluctuation spectroscopy

F. Livet and F. Bley
*LTPCM-ENSEEG-INPG, UMR-CNRS No. 5614, Boîte Postale 75-38402 Saint Martin d'Hères Cedex, France*

R. Caudron
*ONERA-LEM, Boîte Postale 72-29 avenue de la division Leclerc, 92322 Châtillon Cedex, France*
*and Laboratoire Léon Brillouin (CEA-CNRS), CEA Saclay, 91191 Gif-sur-Yvette, France*

E. Geissler
*LSP-UJF, UMR-CNRS No. 5588, Boîte Postale 87-38402 Saint Martin d'Hères Cedex, France*

D. Abernathy, C. Detlefs, and G. Grübel
*ESRF, Boîte Postale 220-38043, Grenoble, France*

M. Sutton
*Centre of the Physics of Materials, McGill University, 3600 University Street, Montreal, PQ, Canada H3A-2T8*
(Received 22 September 2000; published 21 February 2001)

Irreversible decomposition of an AlLi single crystal has been studied by x-ray photon correlation spectroscopy. The precipitate coarsening follows a universal behavior, as measured by the time-resolved average scattering. Using coherent scattering, two-time correlation functions have been measured. The time evolution of the speckle pattern gives new insight into the process of unmixing; at least two regimes govern this evaporation-condensation coarsening process. One is related to the overall arrangement of precipitates, and the characteristic time is linear with annealing time. The other is related to the motion of interfaces and is related to Porod's law.

DOI: 10.1103/PhysRevE.63.036108 PACS number(s): 05.70.Ln, 61.10.Eq, 81.30.Mh, 64.75.+g

## I. INTRODUCTION

Intensity fluctuation spectroscopy is an ideal way to study the kinetics of fluctuations in a system provided that the scattering intensity is sufficient for the time scales of the system under study. For the last three decades or so, it has been extensively used with light scattering to study a large variety of systems [1]. The technique has been recently extended into the x-ray region [2–4] where it has the advantages of accessing opaque materials, of probing shorter length scales and of being less affected by multiple scattering. The prime disadvantage of x-rays over visible light is the much lower intensity levels of x-ray sources.

Although extremely successful for equilibrium systems, intensity fluctuation spectroscopy is not often used to study fluctuations in nonequilibrium systems. The reason for this appears to be the difficulty in how to interpret the intensity fluctuations. For equilibrium systems, the average intensity is constant in time and the fluctuations about this average depend only on the time difference between two measurements. Thus one can use conventional autocorrelation techniques which average over many measurements to obtain data with a high signal to noise ratio. In nonequilibrium systems, things are more difficult since the average intensity varies with time and it is not clear how to separate fluctuations from a changing average. Also for nonequilibrium systems there is no reason to expect that correlations will depend only on the time difference and so a full two-time correlation function should be used.

The development of long range order out of a disordered state that occurs after quenching a system through a phase transition is a common and well studied class of nonequilibrium phenomena. Experiments and theories on these systems have led to the concept of dynamic scaling. This suggests there is typically one time dependent length scale $L$ (for example, an average domain size), which controls the time evolution of these processes. When the system is scaled by this length, it has no other average time dependence. The time dependence of this length scale has a power law, $L \sim t^n$ with growth exponent $n$. The growth exponents depend on only a few properties of the underlying system and since they depend on even fewer properties the critical exponents are often called superuniversal. For example, unlike equilibrium critical exponents of systems near continuous phase transitions, they do not depend on spatial dimensionality. Typical examples of growth exponents are $n=1/2$ for scalar order parameters in nonconserved systems and $n=1/3$ for conserved systems (called model A and model B [5]). Intensity fluctuation spectroscopy gives the possibility of studying the fluctuations about this time averaged behavior.

In a study of phase separation in a sodium borosilicate glass [6] it was shown how to use an area detector and the isotropy of the x-ray scattering to obtain an instantaneous average which can be used to decompose the time evolution of the scattering into an average and a fluctuating component. The predictions of dynamical scaling using this decomposition are given in Refs. [7,8]. These results highlight the different nature of fluctuations in nonequilibrium systems

 

when compared to conventional equilibrium fluctuations and also how these fluctuations scale at long times. A dominant feature is the long lived nature of the fluctuation times which increase with annealing times, a phenomenon called persistence.

In this paper, we present a study of the nonequilibrium fluctuations in an alloy of the Al-Li system. Decomposition kinetics in alloys undergoing an unmixing transition have been extensively studied. Among metal alloys, $Al_{1-x}Li_x$ with $x$ near 9% has proven to be an ideal system in which to study the coarsening regime. This system has been observed by electron microscopy [9,10] and small-angle x-ray scattering [11,12]. Together, these measurements present a consistent view of the process as an average increase of precipitate size with time which appears to closely follow an ideal Lifschitz-Slyosov-Wagner (LSW) [13] evaporation-condensation mechanism. Only one size $L$ is necessary to describe coarsening and scaling holds with $L^3 \propto t$.

## II. EXPERIMENT

### A. Alloy and sample setup

In Al-Li alloys with low Li content, unmixing occurs between a disordered Al-based phase, and an ordered $L1_2$ ($Al_3Li$) phase with spherical precipitates. After the unmixing reaction is complete, the coarsening behavior predicted by LSW controls the late stage growth. Several factors result in highly spherical precipitates even at high volume fractions [14]: each precipitate has only one variant of the $L1_2$ ordered phase so there are no antiphase boundaries [15], Al and Li have similar sizes so the matrix-precipitate interfaces are highly coherent with low elastic energy and the system is far from any critical point.

For this experiment, an Al-9 at. % Li single crystal was annealed for 3 min at 475 C, far above the miscibility gap, and then water quenched to room temperature. The initial state of the sample was not completely disordered, because quenched-in vacancies induce some lithium diffusion at room temperature and lead to the formation of small precipitates. These revert upon subsequent annealing at higher temperature [16]. The sample was thinned by mechanical polishing to a thickness of 100 $\mu$m suitable for performing small-angle scattering measurements in transmission. The surface orientation is (110).

A small vacuum furnace was specially designed for this kind of experiment. Water circulation close to the heater ensures a high thermal ($\sim$0.01 C) and mechanical stability while still giving fast response times. The unmixing kinetics experiment was performed at 220 C. This temperature was chosen in order to obtain precipitate sizes large enough to give a good signal at the small angles used in the coherence measurements (a diameter of 500 Å is reached after about 10 h annealing).

### B. X-ray setup

Experiments were carried out on the ID10 Troika beamline at ESRF. The use of this beamline for coherent x-ray scattering is described in Refs. [17,18]. For this experiment, a Si (111) monochromator was used to select a 8.2 keV ($\lambda = 1.51$ Å) beam from the third harmonic of the undulator. The relative energy width was $1.4\times10^{-4}$ full width at half maximum (FWHM). Higher harmonics of the monochromator were suppressed by means of a small mirror.

A 12 $\mu$m diameter pinhole was used to define a coherent beam. The pinhole-sample distance was 0.15 m and the sample was 45 m from the source. Parasitic scattering from the pinhole was limited by guard slits, set to 20 $\mu$m$\times$20 $\mu$m, positioned halfway between the pinhole and the sample. A direct-illumination deep-depletion charge-coupled device (CCD) (Princeton Instruments) was used as an area detector. Its size is about 8 mm$\times$12 mm, with pixel dimensions of $d=22$ $\mu$m. The sample to detector distance was $R=2.3$ m. The detector arm flight path was evacuated with a fixed 2 mm beamstop placed on its output. During the experiment the detector was translated so that $q$ values up to $2.8\times10^{-2}$ Å$^{-1}$ could be reached.

The CCD detector was used in a photon counting mode. This was done by using a droplet algorithm to identify the regions of charge deposited in the CCD by the incident x-rays and replacing them by integer photon counts [19]. To be able to use this algorithm, it is necessary that these droplets be relatively isolated with at most a few x-rays in each droplet. This algorithm eliminates the electronic noise of each pixel (dark current). Although this dark current is small, its removal is important since at low count rates the noise from hundreds of pixels without x rays can dominate the signal from a few pixels with x rays.

The incident beam intensity was monitored using a small scintillator measuring the scattering of a thin kapton foil located after the beam defining pinhole. The experiment was performed by heating the sample from room temperature to 220 C in under 10 s and spectra were recorded in sets of 2000 frames each of 1.5 s exposure time. Time was recorded for each set with a dead time of 0.26 s/frame for reading the CCD. After being transformed by the ''droplet algorithm'' into individual x rays, either 100 or 200 frames were summed to improve statistics.

X-ray intensity fluctuation measurements typically use only partially coherent light to gain an increase in count rates. This partial coherence can be characterized by a coherence factor $\beta$ which is the decay amplitude of the normalized correlation function. From the source size for the Troika beamline [900 $\mu$m horizontal by 23 $\mu$m vertical ($H\times V$ FWHM)] and the above-mentioned wavelength spread, the transverse coherence area is found to be 6 $\mu$m$\times$220 $\mu$m ($H\times V$ FWHM). At 2.3 m the speckle size corresponds to 23 $\mu$m (FWHM) which is close to the pixel size. Calculation gives an estimated $\beta$ of 0.3 [20,21] which is in good agreement with the measured value from our experiments of 0.25.

## III. RESULTS

### A. Incoherent scattering

First we compare our data to the results predicted by dynamic scaling. Circular averaging of the speckle intensity

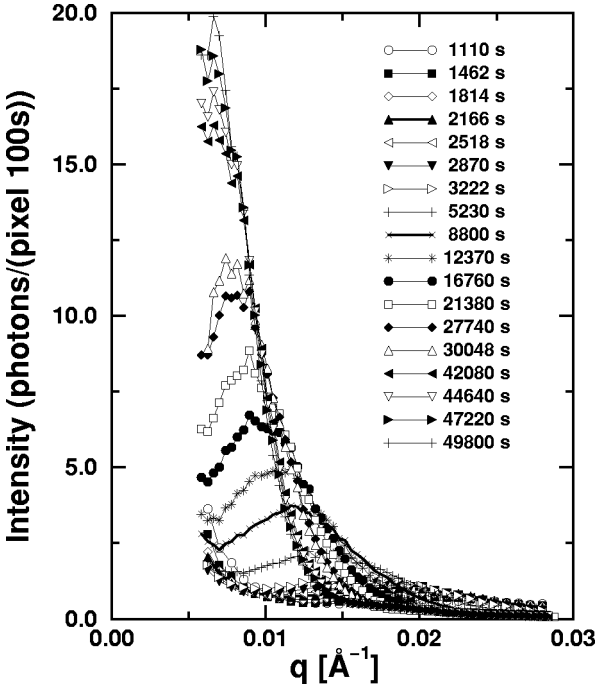


FIG. 1. Time evolution of scattered intensity.

provides a measurement of the incoherent intensity: $I(q,t) = \langle I(\mathbf{q},t)\rangle_{|\mathbf{q}|=\mathbf{q}}$. The 200 000 pixels of the detector were mapped into either 40, 20, or 10 pixel wide circular domains of constant $|\mathbf{q}|$. The number of independent intensities is thus large enough so that no speckle structure is observed in the average. Figure 1 shows the measured intensity evolution. Intensities are plotted for 100 s total counting time, and the evolution is studied for about 14 hours. The data shows a peak in the scattering which grows in intensity with time and shifts to lower $q$. From this data one can measure $q_{\max}(t)$ as the wave vector that gives the maximum intensity at a constant time $t$ and $t_{\max}(q)$ as the time for which the intensity is a maximum at constant $q$. From Fig. 1, it should be noticed that the intensity at $q_{\max}$ for a given time is smaller than the intensity at $t_{\max}$ for a given $q$.

Provided the sample is in the coarsening regime where the chemical unmixing between the matrix and the precipitates has finished, dynamic scaling predicts that the properties of a system should scale with a single characteristic domain size $L$ and that this length scale should grow as $t^{1/3}$. The time evolution of the characteristic domain size $L$ of the sample can be estimated either by the Guinier radius $R_G$ or by $q_{\max}^{-1}$. For both these size estimates, one can see (Fig. 2) the predicted dependence. Scaling also predicts that the peak intensity should grow linearly in time as is also shown in Fig. 2. A stronger test of scaling is given by whether the scattering function itself scales. This scaling is shown for a fixed $q$ as function of $t/t_{\max}$ in Fig. 3, and for a fixed $t$ as a function of $q/q_{\max}$ in Fig. 4.

Figure 4 is presented as a scaled Porod plot which is sensitive to the precise shape and size distribution of the particles. Oscillations of $q^4 I(q)$ around the constant Porod limit are related to the narrow size distribution of spherical

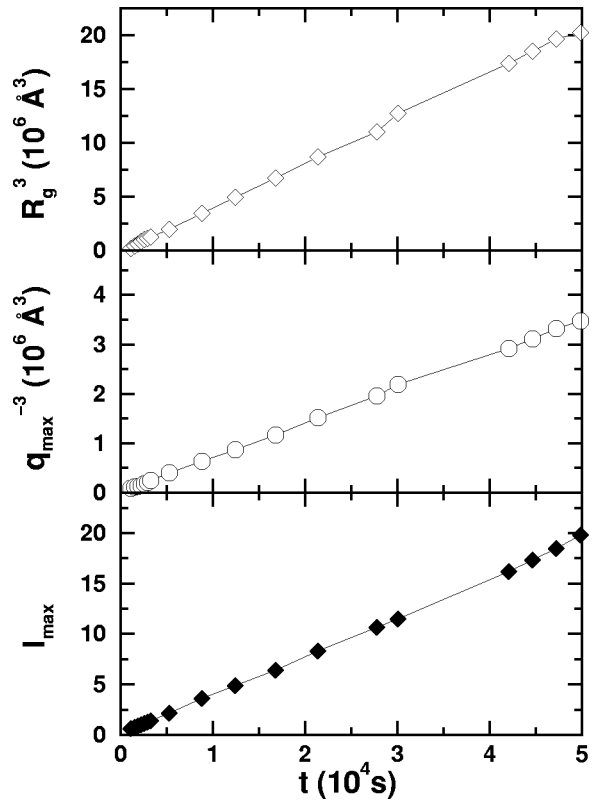


FIG. 2. Coarsening behavior of the system, as shown by $R_g$, $q_{\max}$, and $I_{\max}$.

$Al_3Li$ particles. As no significant change of these oscillations is observed throughout the time evolution studied ($2\pi q_{\max}^{-1}$ varies from 280 to 1000 Å), one can consider that the shape and the scaled size distribution of the $Al_3Li$ particles is not

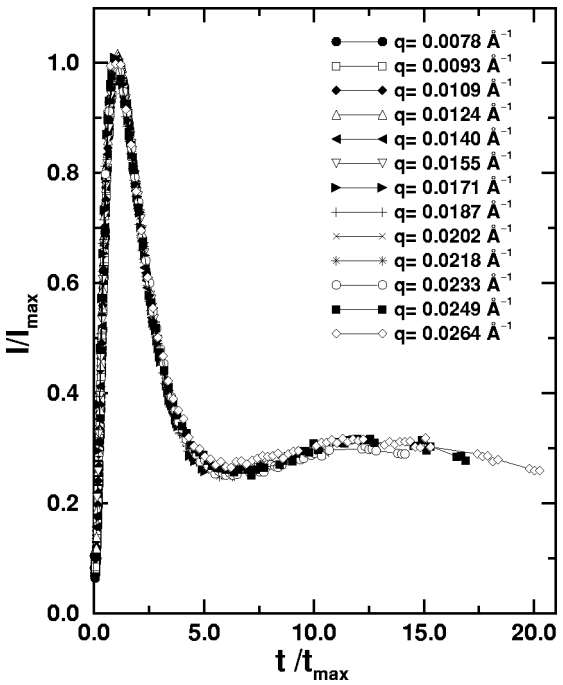


FIG. 3. Scaled intensity vs scaled time for different $q$ values.

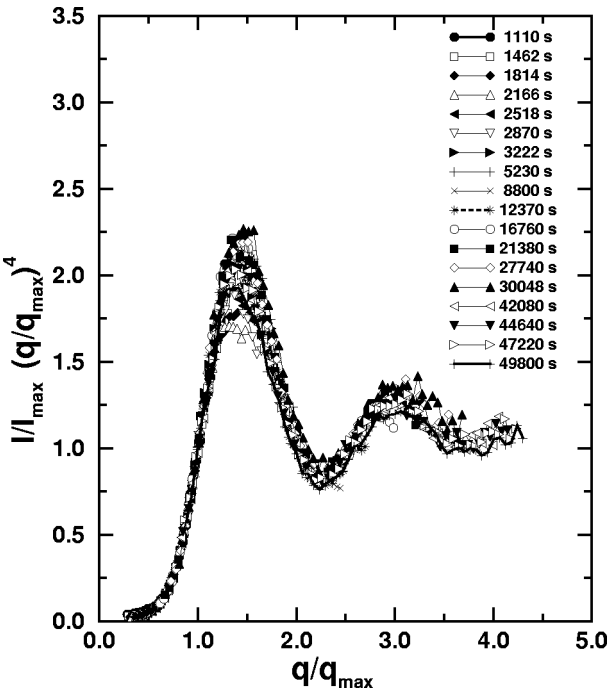


FIG. 4. Scaled Porod function after subtraction of a small constant background.

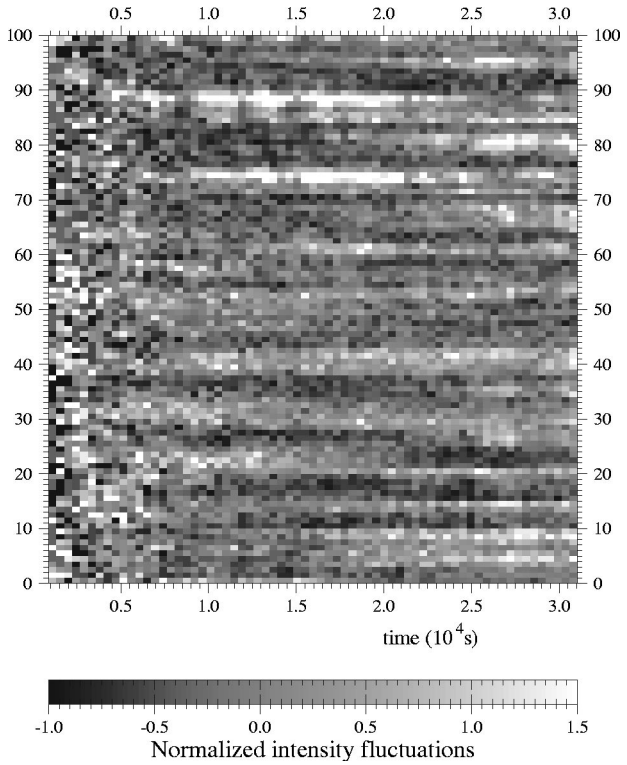


FIG. 5. Time evolution of normalized intensity fluctuations [Eq. (1)] for some pixels in a ring 10 pixels wide, at $q=0.0117$ Å$^{-1}$.

changing greatly with time. For many examples of unmixing processes in crystalline solids (Al-Zn,Ni-Al), the initially spherical precipitates change shape as they grow. For Al-Li the lattice misfit is extremely small, as demonstrated by how difficult it is to observe elastic field contrast by electron microscopy [9]. The present scaling results just reiterate the fact that Al-Li is a good model system for the LSW growth mechanism and this is nicely corroborated by our scattering data.

### B. Intensity fluctuation spectroscopy

In practice, for isotropic systems, an instantaneous average can be calculated by averaging over intensities at constant $q$ as was used to study the scaling behavior in the preceding section. Based on the high degree to which scaling works in the Al-Li system, this is equivalent to studying the fluctuations about an instantaneous ''average'' as determined by the scaling form.

Here we present averages over 40 pixel wide annuli to obtain $\langle I(q,t)\rangle$ but calculations with 20 pixel annuli gave the same result aside from an increased Poisson noise. Since the scattering is isotropic, this average is the instantaneous average intensity at time $t$ for pixel $\mathbf{q}$. A normalized intensity fluctuation can then be defined as

$$D(\mathbf{q},t)=\frac{I(\mathbf{q},t)-\langle I(q,t)\rangle}{\langle I(q,t)\rangle}. \tag{1}$$

This is the relative deviation of coherent intensity with respect to the average incoherent intensity. Typical behavior for our data is seen in Fig. 5 showing the time evolution of $D$ for various pixels with the same $q=0.117$ Å$^{-1}$. It clearly shows the slowing down of the fluctuations with time.

The average of the product of such terms at $t_1$ and $t_2$ gives the two-time correlation function

$$C(q,t_1,t_2)=\langle D(\mathbf{q},t_1)^{*}D(\mathbf{q},t_2)\rangle_{|\mathbf{q}|=q}. \tag{2}$$

For $t_1=t_2$, this function is the sum of a term due to the Poisson noise from photon statistics and one due to the coherence factor $\beta$. As the Poisson noise is only present in the equal time function, it can be removed by extrapolating the values on each side $t\pm\delta t$, $\delta t$ being the time step. To describe its evolution, a normalized two-time correlation function, symmetrical in $t_1$ and $t_2$, is calculated as

$$C_{\mathrm{norm}}(q,t_1,t_2)=\frac{2C(t_1,t_2)}{(C(t_1,t_1-\delta t)+C(t_1,t_1+\delta t))^{1/2}(C(t_2,t_2-\delta t)+C(t_2,t_2+\delta t))^{1/2}} \tag{3}$$

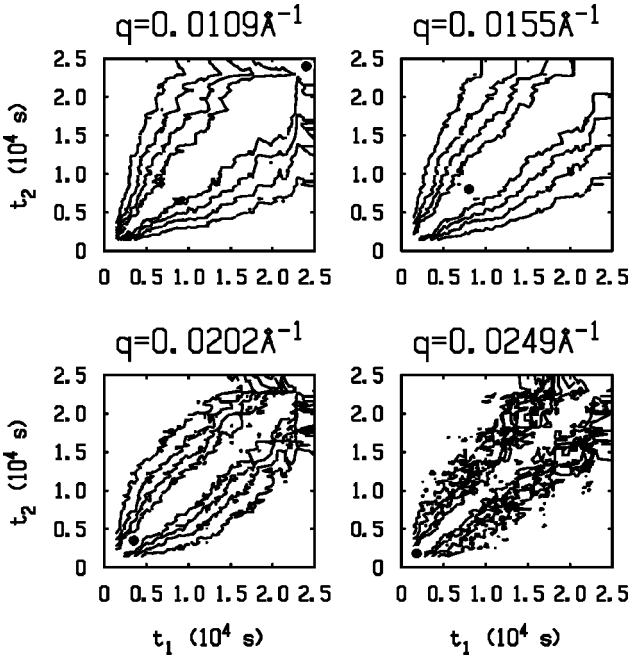


FIG. 6. Contour plots of two-time correlation functions for different $q$ values; contour levels are 0.2, 0.4, 0.6, 0.8. The black dots indicates $t_{max}$ for the given $q$.

The $q$ dependence in $C(q,t_1,t_2)$ has been omitted for simplicity. The two-time correlation function was defined in the same way as Ref. [6].

The intermediate values $[C(q,t_1,t_1-\delta t)+C(q,t_1,t_1+\delta t)]/2$ provide another way to estimate the coherence factor $\beta$; $\beta$ can also be calculated in a more usual way from the angular variations of intensity for time $t$:

$$\beta=\frac{\langle I^2(q,t)\rangle-\langle I(q,t)\rangle}{\langle I(q,t)\rangle^2}-1, \tag{4}$$

where $I(q,t)$ is x-ray counts and the formula corrects for Poisson noise. Both calculations are in agreement and give a value close to 0.25. This result gives the instantaneous coherence. Beam instabilities can affect the two-time correlation function; for example, total decorrelation was observed after a realignment of the beam between times 30 000 and 40 000 s (not shown here), after an injection of the synchrotron. The long term stability of the beam will be discussed later in the paper.

Contours of the normalized two-time correlation function of $t_1$ and $t_2$ are plotted in Fig. 6 for some typical $q$ values [the diagonal $t_1$ equal to $t_2$ is unity by Eq. (3)]. It can be seen that the correlations in this nonequilibrium system depend on both time arguments. For comparison, in an equilibrium system, these correlations would only depend on $t_1-t_2$ and all contours would be parallel to the diagonal. Then one can average over $(t_1+t_2)/2$ to improve statistics. The curves show correlation times that increase with total time but for higher $q$, the contours become more parallel to the diagonal. The black dots in the figure indicate the $t_{max}$ for the given $q$.

It is natural to use the new variables: $\Delta t=t_1-t_2$ and $\bar{t}=(t_1+t_2)/2$ to describe these correlations. For constant

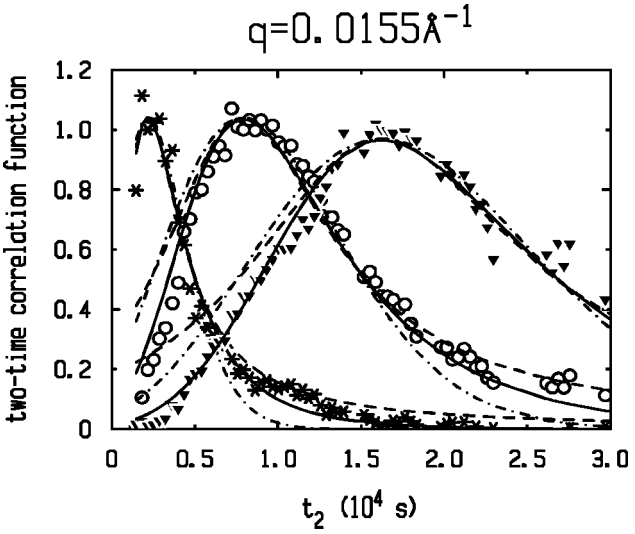


FIG. 7. Correlation function $C_{norm}(q,t_1,t_2)$ for $q=0.0155$ Å$^{-1}$ value and $t_1=2163$ s; 7920 s; 16230 s. Solid lines are the fits to Eq. (5). For comparison, the dashed-dotted line is a Gaussian and dashed line is a Lorentzian with the same height and width.

$\bar{t}$, $C_{norm}$ is a symmetric function of $\Delta t$ that falls monotonically from unity at $\Delta t=0$ to zero at large $\Delta t$. This gives a characteristic correlation time $\tau$, which can be taken as the time at which $C_{norm}$ falls to 0.5. Just as the single time correlation function $I(q,t)$ satisfies dynamic scaling, so do the two-time correlation functions. Based on a moving interface model, an analytical form for this normalized two-time correlation function can be calculated [8]. The form predicted for a three-dimensional system at large $\bar{t}$ is

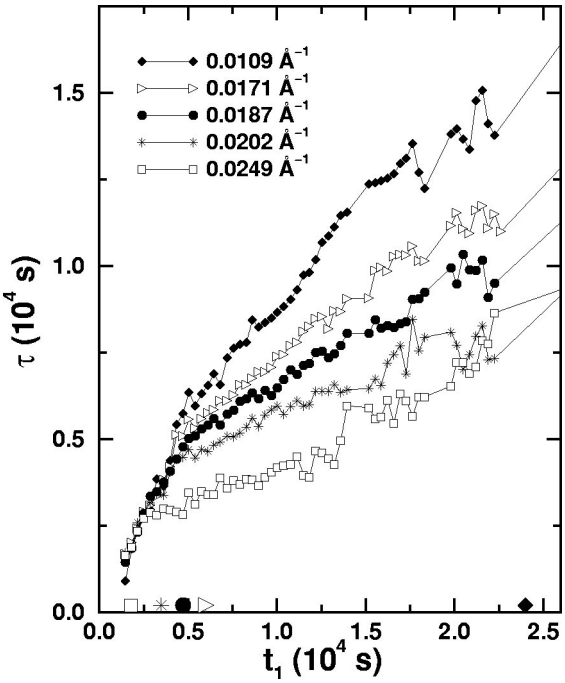


FIG. 8. Fitted correlation times for some $q$ values. The symbols on the lower axis indicate values of $t_{max}$ for the values of $q$ with the same symbol.

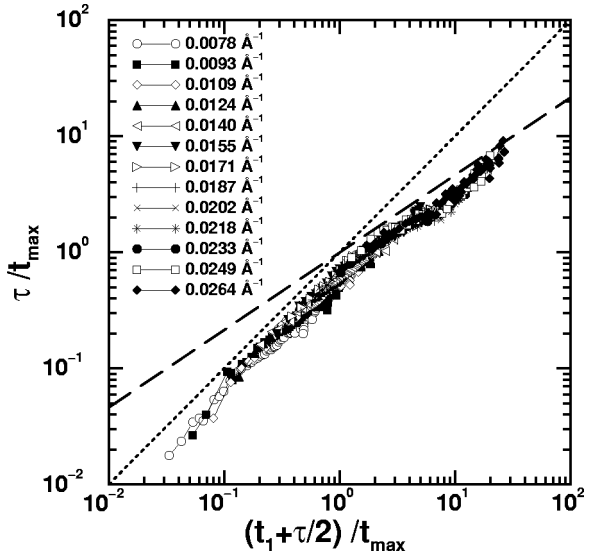


FIG. 9. Scaled fitted correlation times for all $q$ values [using Eq. (5)]. The dotted line has slope 1 and the dashed line has slope 2/3.

$$C_{\mathrm{norm}}(z) = (z^2 K_2(z)/2)^2. \tag{5}$$

$K_2(z)$ is a modified Bessel function of the second kind [22] and the scaling variable is $z = A\Delta t/\overline{t}^{2/3}$, where $A$ makes the variable dimensionless. This form was used to fit the data and determine the half width at half maximum $\tau$. Representative fits are shown in Fig. 7 where the data are plotted as slices at constant $t_1$. This equation strictly only applies for large $\overline{t}$, but as can be seen in the figure, it works well for all times and provides an accurate way of estimating $\tau$. Equally good fits were obtained using $z = \Delta t/\overline{t}$. For comparison, the figure also shows a Lorentzian and a Gaussian functional form. The proposed functional form fits much better. The correlation functions for this system are quite different from the exponential decays typically found in equilibrium systems. Figure 8 shows the correlation times from the resulting fits for several values of $q$. As seen in Fig. 6, the correlation times grow with time from the start of the annealing. Also, it clearly shows that the time scales for smaller wave vectors are correspondingly longer than for larger $q$.

As for the time evolution of the incoherent scattering, the time evolution of the two-time correlation functions should scale at long times. Figure 9 shows the measured correlation times versus $\overline{t}$, scaled by $t_{\mathrm{max}}$. The data collapse quite well onto a universal curve. Theory predicts that this time evolution should have power law dependence in two limits. At early times, but still in the coarsening regime, the correlation time should grow linearly with time and at late times the correlation time should grow as $\overline{t}^{2/3}$. Lines showing these power laws are included on the figure and are consistent with the data. Near $\overline{t}/t_{\mathrm{max}} = 5$ in Fig. 9 there is an inflection point in the universal curve, which corresponds to the local minimum in Fig. 3 at $\overline{t}/t_{\mathrm{max}} = 5$.

Our results agree qualitatively with the theory of Ref. [8]. It is difficult to obtain $t_{\mathrm{max}}$ from their results to make a direct comparison, but quantitative agreement is not expected as the scaling time $t_{\mathrm{max}}$ depends on the volume fractions of the phases and on any asymmetry in the miscibility curve.

Figure 9 indirectly shows the stability of the experimental setup. During the first 9 hours of measurement, a unique universal curve for time correlations is seen for low $q$ as well as for high $q$ values. After the beam was realigned, the correlation functions must be truncated. The different beam positions on the sample mean the speckle patterns cannot be compared.

## IV. DISCUSSION

The Al-Li alloy in the coarsening regime closely follows a universal behavior. In Fig. 8, it is clear that during the coarsening process, the persistence time $\tau$ of the speckles is higher for the smallest $q$ values, i.e., for the largest sizes. Each curve displays only a part of the whole $\tau$ versus $t$ variation, and has some scatter, which is less visible when all curves are gathered after scaling as in Fig. 9. For times less than $\sim 2t_{\mathrm{max}}$, the time dependence of $\tau$ is linear and $\tau$ is of the same order of magnitude of the overall aging time. This occurs for times until just after the peak intensity sweeps by. This peak is related to correlations in precipitate positions for which the speckle pattern corresponds to the relative positions of the larger precipitates. In a LSW process, the relative positions of large precipitates does not change much whereas small precipitates evaporate as their atoms condense on larger ones. Thus the reorganization time of precipitates is proportional to aging time.

At higher reduced times, the universal curve is related to the asymptotic part of intensity, which reflects the interface behavior. After a plateau which corresponds to the first minimum in a Porod representation, the increase of $\tau$ is slowed, with a variation that is compatible with the prediction $\tau \propto \overline{t}^{2/3}$ [8]. This prediction is related to Porod's law and so reflects interface fluctuations in the precipitates during coarsening.

Following the arguments in Ref. [8] similar results should hold whenever scaling applies. Scaling of one time correlation functions gives a characteristic length $L(t)$ that scales as $t^n$ and reflects domain growth. Scaling of two-time correlation functions gives at early times $\tau$ growing linearly in time and, for late times, scaling like $\overline{t}^{1-n}$, reflecting persistence of the fluctuations. It would be most interesting to check these conclusions in other systems. We would also like to point out that even if a system does not follow a scaling law, the procedure for analyzing the data following Eqs. (1)–(3) is still valid. So, it would also be interesting to use either dynamic light scattering or coherent x-ray scattering to see what further insight into the time evolution of such systems can be obtained.

## ACKNOWLEDGMENTS

We acknowledge the European Synchrotron Radiation Facility for provision of their facilities and we would like to thank P. Feder and H. Gleyzolle for technical support at beamline ID10A.

[1] *Dynamic Light Scattering*, edited by W. Brown (Clarendon, Oxford, 1993).
[2] M. Sutton, S. E. Nagler, S. G. Mochrie, T. Greytak, L. E. Bermann, G. Held, and G. B. Stephenson, Nature (London) **352**, 608 (1991).
[3] S. Brauer, G. B. Stephenson, M. Sutton, R. Brüning, E. Dufresne, S. G. J. Mochrie, G. Grübel, J. Als-Nielsen, and D. L. Abernathy, Phys. Rev. Lett. **74**, 2010 (1995).
[4] T. Thurn-Albrecht, W. Steffen, A. Patkowski, G. Meier, E. W. Fischer, G. Grübel, and D. L. Abernathy, Phys. Rev. Lett. **77**, 5437 (1996).
[5] P. C. Hohenberg and B. I. Halperin, Rev. Mod. Phys. **49**, 435 (1977).
[6] A. Malik, A. R. Sandy, L. B. Lurio, G. B. Stephenson, S. G. J. Mochrie, I. McNulty, and M. Sutton, Phys. Rev. Lett. **81**, 5832 (1998).
[7] G. Brown, P. A. Rikvold, M. Sutton, and M. Grant, Phys. Rev. E **56**, 6601 (1997).
[8] G. Brown, P. A. Rikvold, M. Sutton, and M. Grant, Phys. Rev. E **60**, 5151 (1999).
[9] B. Noble and G. E. Thompson, Met. Sci. J. **5**, 114 (1971).
[10] D. B. Williams and J. W. Edington, Met. Sci. , **9**, 529 (1975).
[11] G. Cocco, G. Fagherazzi, and L. Schiffini, J. Appl. Crystallogr. **10**, 325 (1977).
[12] F. Livet and D. Bloch, Scr. Metall. **19**, 1147 (1985).
[13] I. M. Lifschitz and V. V. Slyosov, J. Phys. Chem. Solids **19**, 35 (1961); C. Wagner, Z. Elektrochem. **65**, 581 (1961).
[14] F. Livet, P. Gomiero, and F. Bley, Scr. Metall. Mater. **23**, 1937 (1989).
[15] H. J. Leamy, P. Schwellinger, and H. Warlimont, Acta Metall. **18**, 31 (1970).
[16] F. Livet and Y. Bréchet, J. Phys. (Paris) **48**, C3-357 (1987).
[17] D. L. Abernathy, G. Grübel, S. Brauer, I. McNulty, G. B. Stephenson, S. G. J. Mochrie, A. R. Sandy, N. Mulders, and M. Sutton, J. Synchrotron Radiat. **5**, 37 (1998).
[18] J. Mainville, F. Bley, F. Livet, E. Geissler, J. F. Legrand, D. L. Abernathy, G. Grübel, S. G. J. Mochrie, and M. Sutton, J. Appl. Crystallogr. **30**, 828 (1997).
[19] F. Livet, F. Bley, J. Mainville, M. Sutton, R. Caudron, S. G. J. Mochrie, E. Geissler, G. Dolino, D. L. Abernathy, and G. Grübel, Nucl. Instrum. Methods Phys. Res. A **451**, 596 (2000).
[20] F. Livet, F. Bley, A. Létoublon, J. P. Simon, and J. F. Bérar, J. Synchrotron Radiat. **5**, 1337 (1998).
[21] A. R. Sandy, L. B. Lurio, S. G. J. Mochrie, A. Malik, G. B. Stephenson, J. F. Pelletier, and M. Sutton, J. Synchrotron Radiat. **6**, 1174 (1999).
[22] This scaling form can be further approximated by $C_{\mathrm{norm}}(z) \cong e^{-2z}(1+z+z^2/4-z^3/12)^2$ which is valid for $z<3$. Solving numerically gives $C_{\mathrm{norm}}(z=1.2579)=0.5$.